

Experimental and theoretical study of polarized photoluminescence caused by anisotropic strain relaxation in nonpolar a-plane textured ZnO grown by a low-pressure chemical vapor deposition

Chih-Ming Lai, Yu-En Huang, Kuang-Yang Kou, Chien-Hsun Chen, Li-Wei Tu, and Shih-Wei Feng

Citation: *Applied Physics Letters* **107**, 022110 (2015); doi: 10.1063/1.4926978

View online: <http://dx.doi.org/10.1063/1.4926978>

View Table of Contents: <http://scitation.aip.org/content/aip/journal/apl/107/2?ver=pdfcov>

Published by the [AIP Publishing](#)

Articles you may be interested in

[Enforced c-axis growth of ZnO epitaxial chemical vapor deposition films on a-plane sapphire](#)

Appl. Phys. Lett. **100**, 182101 (2012); 10.1063/1.4709430

[Development of tilted hexagonal platelet ZnO using atmospheric pressure chemical vapor deposition and investigation of its growth mechanism](#)

Appl. Phys. Lett. **100**, 061909 (2012); 10.1063/1.3681163

[Texture vs morphology in ZnO nano-rods: On the x-ray diffraction characterization of electrochemically grown samples](#)

J. Appl. Phys. **110**, 124901 (2011); 10.1063/1.3669026

[Self-limiting deposition of semiconducting ZnO by pulsed plasma-enhanced chemical vapor deposition](#)

J. Vac. Sci. Technol. A **27**, 761 (2009); 10.1116/1.3119673

[Growth of ZnO films on R -plane sapphire substrates by atmospheric-pressure chemical vapor deposition using Zn powder and H₂O as source materials](#)

J. Vac. Sci. Technol. B **27**, 1646 (2009); 10.1116/1.3130157

A promotional banner for COMSOL software. On the left, a white box contains the text 'LIVE DEMO' and 'The Basics of COMSOL in 18 Minutes'. The COMSOL logo is at the bottom left. The background features a 3D bar chart with colorful, flowing lines representing data or simulation results. A blue button with the text 'REGISTER >>' is located in the top right corner.

Experimental and theoretical study of polarized photoluminescence caused by anisotropic strain relaxation in nonpolar *a*-plane textured ZnO grown by a low-pressure chemical vapor deposition

Chih-Ming Lai,¹ Yu-En Huang,² Kuang-Yang Kou,³ Chien-Hsun Chen,⁴ Li-Wei Tu,⁵ and Shih-Wei Feng^{2,a)}

¹Department of Electronic Engineering, Ming Chuan University, Taoyuan 333, Taiwan

²Department of Applied Physics, National University of Kaohsiung, Kaohsiung 811, Taiwan

³Department of Traffic Science, Central Police University, Taoyuan 333, Taiwan

⁴Green Energy and Environment Research Labs, Industrial Technology Research Institute, Hsinchu 310, Taiwan

⁵Department of Physics and Center for Nanoscience and Nanotechnology, National Sun Yat-Sen University, Kaohsiung 804, Taiwan

(Received 26 March 2015; accepted 6 July 2015; published online 15 July 2015)

Anisotropic strain relaxation and the resulting degree of polarization of photoluminescence (PL) in nonpolar *a*-plane textured ZnO are experimentally and theoretically studied. A thicker nonpolar *a*-plane textured ZnO film enhances the anisotropic in-plane strain relaxation, resulting in a larger degree of polarization of PL and better sample quality. Anisotropic in-plane strains, sample quality, and degree of polarization of PL in nonpolar *a*-plane ZnO are consequences of the degree of anisotropic in-plane strain relaxation. By the *k*-*p* perturbation approach, simulation results of the variation of the degree of polarization for the electronic transition upon anisotropic in-plane strain relaxation agree with experimental results. © 2015 AIP Publishing LLC.

[<http://dx.doi.org/10.1063/1.4926978>]

Wide-band-gap wurtzite zinc oxide (ZnO) semiconductor is a very promising material for optoelectronic applications in the ultraviolet (UV) range.^{1–6} ZnO grown along the polar *c*-axis experiences piezoelectric and spontaneous polarizations, in which quantum confined Stark effect (QCSE) spatially separates the electrons and holes in the quantum wells and decreases device efficiency.^{4–6} Nonpolar ZnO grown along the *m*- and *a*-axes can reduce the QCSE and enhance the radiative efficiency of light emitting diodes (LEDs).^{4–6}

For nonpolar *a*-plane ZnO, the large anisotropic difference of lattice mismatch and expansion coefficient between the film and substrate on the growth plane result in anisotropic in-plane strains and distortion of the hexagonal unit cells.^{7–10} The in-plane anisotropic strains break the crystal symmetry and modify the valence band structures from the unstrained $|X \pm iY\rangle$ heavy hole and light hole states into $|X\rangle$ – like and $|Y\rangle$ – like states, leading to anisotropic optical properties.^{7–10} In addition, polarized emission in non-polar *a*-plane gallium nitride (GaN) attributed to anisotropic in-plane strain has also been observed.¹¹ The phenomenon has been identified by strain-dependent electronic band structure modification through the *k*-*p* perturbation approach.¹¹ The oscillator strength and degree of polarization of the electronic transition have been shown to strongly depend on the in-plane strains. Although the argument of valence band structure modification has been adopted to qualitatively explain the polarized optical properties in nonpolar *a*-plane ZnO, electronic band structures are not theoretically calculated in terms of the in-plane strains. In particular, the

variation of the degree of polarization of electronic transition upon anisotropic strain relaxation in nonpolar *a*-plane ZnO is not well discussed.

This study reports anisotropic strain relaxation and the resulting degree of polarization in nonpolar *a*-plane ZnO. A thicker nonpolar *a*-plane ZnO film enhances the anisotropic in-plane strain relaxation, resulting in a larger degree of polarization of photoluminescence (PL) and better sample quality. By the *k*-*p* perturbation approach, simulation results of electronic band structures show that the oscillator strength and degree of polarization of the electronic transition strongly depend on the in-plane strains. The variation of the degree of polarization of electronic transition upon anisotropic strain relaxation agrees with the experimental results.

The nonpolar *a*-plane ZnO samples were grown on an *r*-sapphire substrate at 170 °C with a pressure of 0.6 Torr in a low-pressure chemical vapor deposition (LPCVD) reactor. Diethyl zinc (DEZ) and water (H₂O) were used as the precursors for the Zn and O, respectively. H₂O was in a vapor form. ZnO thin film was doped with boron (B) to improve the electrical transport properties.¹² Three nonpolar *a*-plane ZnO: B samples with 20-, 40-, and 60-min growth times, corresponding to 270, 540, and 1000 nm in thickness, were prepared (namely, *a*-20, *a*-40, and *a*-60 samples, respectively). For the three samples, the B₂H₆, DEZ, and H₂O flow rates were 1, 500, and 550 sccms, respectively.

High-resolution *x*-ray diffraction (XRD) was taken to confirm the evidence of *a*-plane ZnO samples. Polarized Raman spectra were taken to estimate the in-plane strains using a Jobin Yvon-Horiba micro-Raman system (model T64000) with a 532 nm laser. The samples were placed in a cryostat for low-temperature (10 K) PL measurement with the 266 nm line of an Nd:YAG pulse laser for excitation.

^{a)}Author to whom correspondence should be addressed. Electronic mail: swfeng@nuk.edu.tw

The pulse laser had a pulse width of 10 ns and a repetition rate of 20 Hz. The PL polarization was analyzed using an UV polarizer in front of the spectrometer.

Figure 1 shows the polarized Raman scattering spectra under $x(yy)\bar{x}$ configuration. The two dotted lines (379.0 and 439.0 cm^{-1}) show the phonon frequencies $A_1(\text{TO})$ and $E_2\text{-high}$, respectively, for strain-free ZnO. The frequency shifts $\Delta\omega = (\omega - \omega_0)$ can be described as a function of in-plane strains ε_{yy} and ε_{zz} (Ref. 13)

$$\Delta\omega(A_1(\text{TO})) = 2a\varepsilon_{yy} + b\varepsilon_{zz} = 2(-774)\varepsilon_{yy} - 375\varepsilon_{zz}, \quad (1)$$

$$\Delta\omega(E_2(\text{High})) = 2a\varepsilon_{yy} + b\varepsilon_{zz} = 2(-580)\varepsilon_{yy} - 765\varepsilon_{zz}, \quad (2)$$

where $a = -774$ and -375 cm^{-1} and $b = -580$ and -765 cm^{-1} are the deformation potential constants for $A_1(\text{TO})$ and $E_2(\text{high})$ modes, respectively.¹³ $A_1(\text{TO})$ and $E_2(\text{high})$ modes were chosen to estimate the in-plane strains ε_{yy} and ε_{zz} in calculating Eqs. (1) and (2).

As shown in Table I, as the thickness increases, both the in-plane tensile strain ε_{yy} and in-plane compressive strain ε_{zz} decrease, showing an anisotropic strain relaxation. The trend of the fast strain relaxation along the y -axis for large misfits and incomplete strain relaxation along the z -axis for small misfits is consistent with that obtained from high-resolution transmission electron microscopy and XRD.^{8,9} These different relaxation processes can be explained in terms of *domain matching epitaxy* and *lattice matching epitaxy* models.^{8,9,14} For the large initial mismatch along the y -axis in a -plane ZnO, a plastic relaxation through nucleation and glide of dislocations is effective because slip systems can easily be activated in this direction, resulting in a very low residual strain. This orientation configuration can be described by the *domain matching epitaxy* model. Also, along the z -axis with low initial mismatch, the relaxation is only partial due to a lack of activated systems. The *lattice matching epitaxy* model, in which the relaxation is driven by nucleation and glide of dislocations beyond the critical thickness, shows this. In addition, larger anisotropic in-plane strains in the sample a -20 reveal unrelieved lattice strains and high sheet resistance, while a larger anisotropic strain relaxation in the

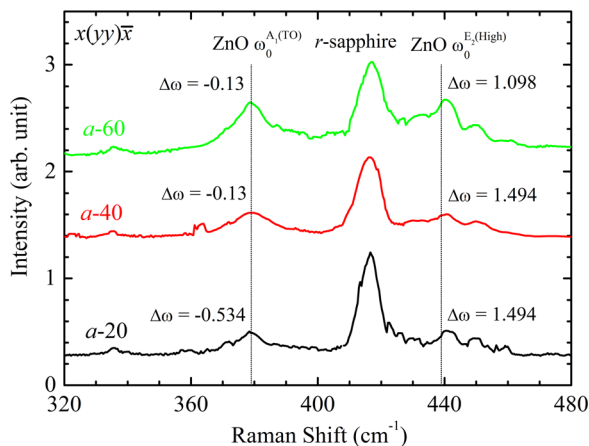


FIG. 1. Polarized Raman scattering spectra for the three a -plane ZnO samples under $x(yy)\bar{x}$ configuration. The Cartesian axes x , y , and z correspond to the $[11\bar{2}0]$, $[1100]$, and $[0001]$ directions of ZnO, respectively. $\Delta\omega(A_1(\text{TO}))$ and $\Delta\omega(E_2(\text{High}))$ for each sample are labeled.

TABLE I. Estimated in-plane strains ε_{yy} and ε_{zz} , sheet resistance (R_{sheet}), and degree of polarization (ρ) for the three a -plane ZnO samples.

Sample	$\varepsilon_{yy}(\%)$	$\varepsilon_{zz}(\%)$	$R_{\text{sheet}}(\Omega/\square)$	ρ
a -20	0.1293	-0.3914	152	0.6751
a -40	0.0881	-0.3288	58.7	0.7112
a -60	0.0682	-0.2470	2	0.7234

sample a -60 is consistent with the lowest sheet resistance. Because the sheet resistance can be expressed as the resistivity divided by film thickness,¹⁵ sheet resistance in thicker and more relaxed ZnO layers becomes lower.

Figures 2(a)–2(c) show the polarized PL spectra with detected polarizations along the y - and z -axes for samples a -20, a -40, and a -60, respectively, at 10 K. The emission peaks around 370 and 450 nm are associated with the overlapped emission components consisting of donor-acceptor pairs and free-to-bound transition and related to a deep level or trap state, respectively.² For the thickest a -60 sample, the larger anisotropic strain relaxation improves the sample quality and enhances the PL intensity. In addition, the PL spectra show a large polarization anisotropy. The degree of polarization, ρ , is defined as¹²

$$\rho = \frac{I_y - I_z}{I_y + I_z}, \quad (3)$$

where I_y and I_z are the PL intensities polarized along the y - and z -axes, respectively. Using a thicker film, the larger anisotropic strain relaxation modifies the electronic band structures and results in a larger degree of polarization of PL. The degree of polarization of PL emission of the c -plane

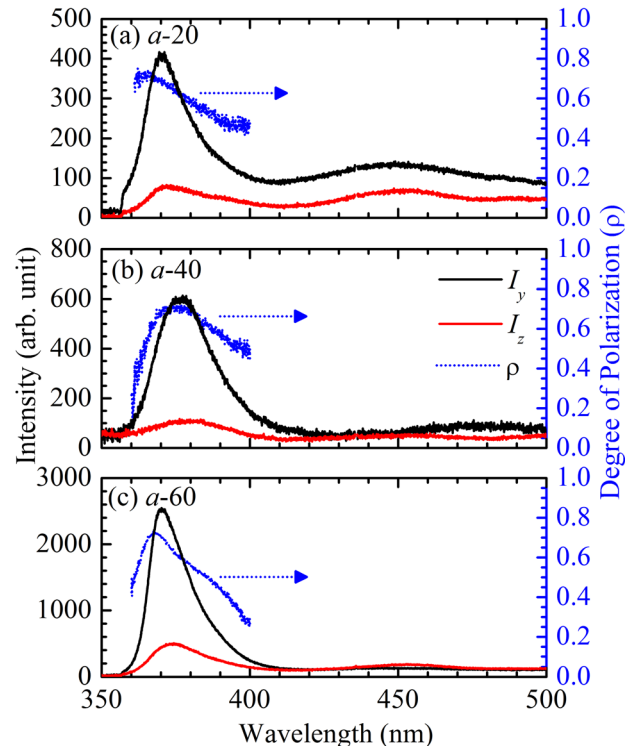


FIG. 2. PL spectra with polarizations along y - and z -axes (left coordinate) and degree of polarization (right coordinate) for samples (a) a -20, (b) a -40, and (c) a -60 at 10 K.

wet-etched InGaN LEDs is not significantly changed by the textured surface.¹⁶ The degree of polarization of PL in *a*-plane ZnO should be maintained even when passed through the textured surface layer. Similar to nonpolar *a*-plane GaN in our previous study,¹¹ it is suggested that anisotropic in-plane strains, sample quality, and degree of polarization of PL in nonpolar *a*-ZnO are consequences of the degree of anisotropic strain relaxation.

By using the *k*-p perturbation approach to simulate the electronic band of nonpolar *a*-plane ZnO, the transition energy, oscillator strength, and degree of polarization from the conduction band to the highest (E_1), second highest (E_2), and third highest (E_3) valence bands are calculated in terms of anisotropic in-plane strains ε_{yy} and ε_{zz} .^{11,17} The material parameters of ZnO, such as energy parameters, valence band deformation potentials, and elastic stiffness constants, are adopted from Refs. 18 and 19. Simulations are performed using in-house code written for Matlab software.

Simulation results of transition energies for (a) E_1 , (b) E_2 , (c) E_3 transitions, and (d) energy difference $E_2 - E_1$ as a function of in-plane strains ε_{yy} and ε_{zz} are shown in Figure 3. In general, the variation of the transition energy along the *y*-direction is larger than that along the *z*-direction. In other words, ε_{yy} is a more important parameter than ε_{zz} in determining the transition energy. Also, the transition energies for $\varepsilon_{yy} > 0$ in quadrants I and II are higher than those for $\varepsilon_{yy} < 0$ in quadrants III and IV.

Figure 4 shows the contour plots of the *x*, *y*, and *z* components of the oscillator strengths for the E_1 , E_2 , and E_3 transitions as a function of in-plane strains ε_{yy} and ε_{zz} . The oscillator strengths of the *x* and *y* components for the E_1 and E_2 transitions show a larger variation of in-plane strains, while the others show smaller ones. Under anisotropic strain relaxation, the large-varied *y* component of the oscillator strengths as a function of in-plane strains will lead to a larger variation of degree of polarization for the E_1 and E_2 transitions.

The degree of polarization ρ can be expressed as follows:¹¹

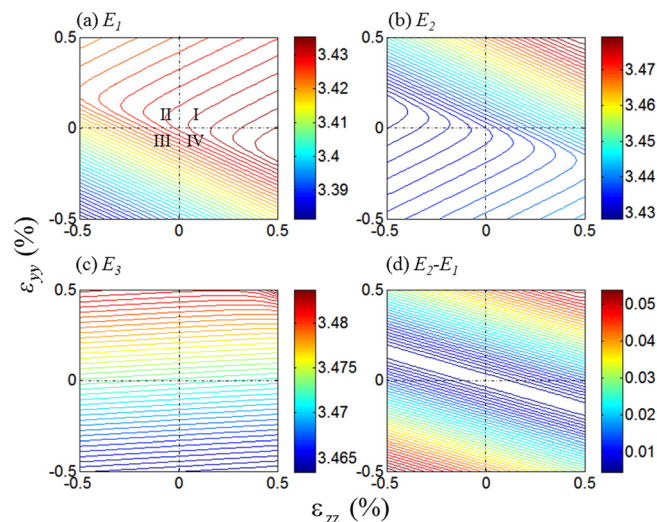


FIG. 3. Simulation result of transition energies (a) E_1 , (b) E_2 , (c) E_3 , and (d) energy difference $E_2 - E_1$ as a function of the in-plane strains ε_{yy} and ε_{zz} of nonpolar *a*-plane ZnO.

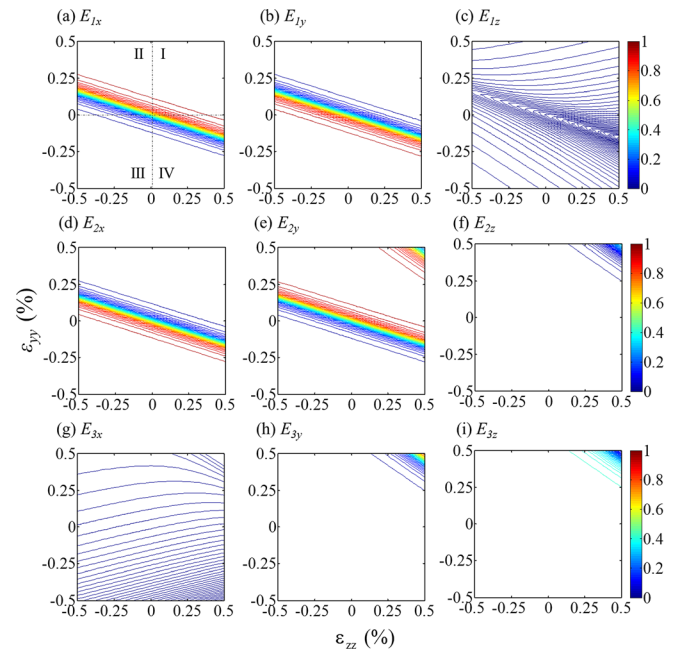


FIG. 4. Relative *x*, *y*, and *z* components of the oscillator strengths of the E_1 [(a), (b), and (c)], E_2 [(d), (e), and (f)], and E_3 [(g), (h), and (i)] transitions as a function of in-plane strains ε_{yy} and ε_{zz} for nonpolar *a*-plane GaN, respectively.

$$\rho = \frac{I_y - I_z}{I_y + I_z} = \frac{\text{Oscillator strength}_y - \text{Oscillator strength}_z}{\text{Oscillator strength}_y + \text{Oscillator strength}_z}. \quad (4)$$

Figures 5(a)–5(d) show the simulation results of the degree of polarization for the E_1 , E_2 , E_3 , and $E_1 + E_2 + E_3$ transitions, respectively, as a function of in-plane strains ε_{yy} and ε_{zz} . Simulation results provide much information about the degree of polarization under anisotropic in-plane strain relaxation in nonpolar *a*-plane ZnO. For the observed anisotropic in-plane strains in quadrant II ($\varepsilon_{yy} > 0$ and $\varepsilon_{zz} < 0$) of Figs. 5(a)–5(d), the degree of polarization for the E_1 , E_2 , and $E_1 + E_2 + E_3$ transitions can be very high (strongly polarized), while that for the E_3 transition is small (weakly polarized).

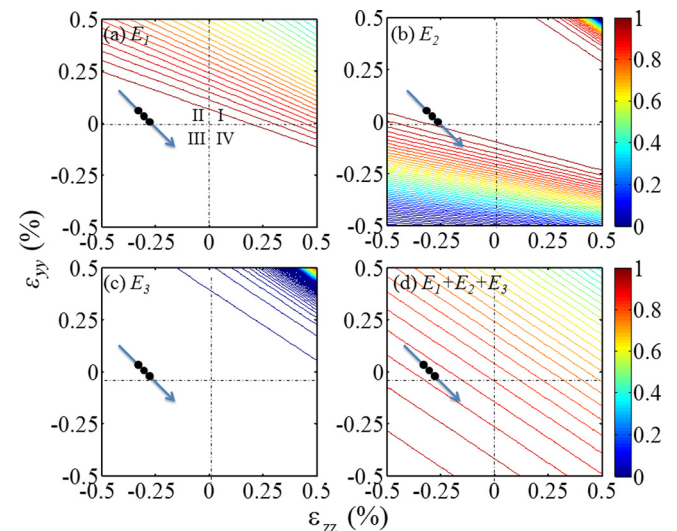


FIG. 5. The degree of polarization for (a) E_1 , (b) E_2 , (c) E_3 , and (d) $E_1 + E_2 + E_3$ transitions as a function of in-plane strains ε_{yy} and ε_{zz} . Arrow indicates the evolution of in-plane strains as the thickness of the film increases.

For the E_1 and $E_1 + E_2 + E_3$ transitions, the degree of polarization increases a little upon anisotropic in-plane strain relaxation within quadrant II (indicated by arrows). Under low excitation, PL may be dominated by the E_1 transition. As shown in Table I, the degree of polarization for the sample a -60 is a little larger. The simulation results of the degree of polarization for the E_1 and $E_1 + E_2 + E_3$ transitions agree with the experimental results.

In summary, it is suggested that anisotropic in-plane strains, degree of polarization of PL, and sample quality in nonpolar a -ZnO are consequences of the degree of anisotropic strain relaxation. The mechanism of anisotropic strain relaxation provides important information for optimized growth of nonpolar ZnO with less lattice misfit strain. The simulation results of the k-p perturbation approach provide much information about transition energy, the oscillator strength, and degree of polarization under anisotropic in-plane strain relaxation in nonpolar a -plane ZnO.

This research was supported by the Ministry of Science and Technology, Taiwan, R.O.C., under Grant No. MOST 103-2112-M-390-002.

¹H. Morkoç and Ü. Özgür, *Zinc Oxide: Fundamentals, Materials and Device Technology* (Wiley-Vch, Weinheim, 2007).

²Ü. Özgür, Ya. I. Alivov, C. Liu, A. Teke, M. A. Reshchikov, S. Doğan, V. Avrutin, S. J. Cho, and H. Morkoç, *J. Appl. Phys.* **98**, 041301 (2005).

- ³A. A. Chaaya, R. Viter, M. Bechelany, Z. Alute, D. Ertz, A. Zaleskaya, K. Kovalevskis, V. Rouessac, V. Smyntyna, and P. Miele, *Beilstein J. Nanotechnol.* **4**, 690 (2013).
- ⁴L. Béaur, T. Bretagnon, C. Brimont, T. Guillet, B. Gil, D. Tainoff, M. Teisseire, and J. M. Chauveau, *Appl. Phys. Lett.* **98**, 101913 (2011).
- ⁵T. Makino, Y. Segawa, M. Kawasaki, and H. Koinuma, *Semicond. Sci. Technol.* **20**, S78 (2005).
- ⁶S. Yang, H. C. Hsu, W. R. Liu, B. H. Lin, C. C. Kuo, C. H. Hsu, M. O. Eriksson, P. O. Holtz, and W. F. Hsieh, *Appl. Phys. Lett.* **105**, 011106 (2014).
- ⁷H. Matsui and H. Tabata, *Appl. Phys. Lett.* **101**, 231901 (2012).
- ⁸G. Saraf, Y. Lu, and T. Siegrist, *Appl. Phys. Lett.* **93**, 041903 (2008).
- ⁹P. Pant, J. D. Budai, and J. Narayan, *Acta Mater.* **58**, 1097 (2010).
- ¹⁰Y. S. Nam, S. W. Lee, K. S. Baek, S. K. Chang, J. H. Song, J. H. Song, S. K. Han, S. K. Hong, and T. Yao, *Appl. Phys. Lett.* **92**, 201907 (2008).
- ¹¹S. W. Feng, Y. Y. Chen, C. M. Lai, L. W. Tu, and J. Han, *J. Appl. Phys.* **114**, 233103 (2013).
- ¹²X. D. Liu, E. Y. Jiang, and Z. Q. Li, *J. Appl. Phys.* **102**, 073708 (2007).
- ¹³G. Callsen, J. S. Reparaz, M. R. Wagner, R. Kirste, C. Nenstiel, A. Hoffmann, and M. R. Phillips, *Appl. Phys. Lett.* **98**, 061906 (2011).
- ¹⁴J. M. Chauveau, P. Vennéguès, M. Lügt, C. Deparis, J. Zuniga-Perez, and C. Morhain, *J. Appl. Phys.* **104**, 073535 (2008).
- ¹⁵H. C. Wang, C. C. Wang, S. W. Feng, L. H. Chen, and Y. S. Lin, *Opt. Mater. Express* **3**, 54 (2013).
- ¹⁶M. Ma, A. N. Noemaun, J. Cho, E. F. Schubert, G. B. Kim, and C. Sone, *Opt. Express* **20**, 16677 (2012).
- ¹⁷S. Ghosh, P. Waltereit, O. Brandt, H. T. Grahn, and K. H. Ploog, *Phys. Rev. B* **65**, 075202 (2002).
- ¹⁸Q. Yan, P. Rinke, M. Winkelkemper, A. Qteish, D. Bimberg, M. Scheffler, and C. G. Van de Walle, *Semicond. Sci. Technol.* **26**, 014037 (2011).
- ¹⁹W. J. Fan, A. P. Abiyasa, S. T. Tan, S. F. Yu, X. W. Sun, J. B. Xia, Y. C. Yeo, M. F. Li, and T. C. Chong, *J. Cryst. Growth* **287**, 28 (2006).